Rab7 Silencing Prevents μ-Opioid Receptor Lysosomal Targeting and Rescues Opioid Responsiveness to Strengthen Diabetic Neuropathic Pain Therapy

Shaaban A. Mousa,[1] Mohammed Shaqura,[1] Baled I. Khalefa,[1] Christian Zöllner,[2] Laura Schaad,[1] Jonas Schneider,[1] Toni S. Shippenberg,[3†] Jan F. Richter,[4] Rainer Hellweg,[5] Mehdi Shakibaei,[6] and Michael Schäfer[1]

Painful diabetic neuropathy is poorly controlled by analgesics and requires high doses of opioids, triggering side effects and reducing patient quality of life. This study investigated whether enhanced Rab7-mediated lysosomal targeting of peripheral sensory neuron μ-opioid receptors (MORs) is responsible for diminished opioid responsiveness in rats with streptozotocin-induced diabetes. In diabetic animals, significantly impaired peripheral opioid analgesia was associated with a loss in sensory neuron MOR and a reduction in functional MOR G-protein-coupling. In control animals, MORs were retained mainly on the neuronal cell membrane. In contrast, in diabetic rats, they were colocalized with upregulated Rab7 in LampI-positive perinuclear lysosome compartments. Silencing endogenous Rab7 with intrathecal Rab7-siRNA or, indirectly, by reversing nerve growth factor deprivation in peripheral sensory neurons not only prevented MOR targeting to lysosomes, restoring their plasma membrane density, but also rescued opioid responsiveness toward better pain relief. These findings elucidate in vivo the mechanisms by which enhanced Rab7 lysosomal targeting of MORs leads to a loss in opioid antinociception in diabetic neuropathic pain. This is in contrast to peripheral sensory neuron MOR upregulation and antinociception in inflammatory pain, and provides intriguing evidence that regulation of opioid responsiveness varies as a function of pain pathogenesis. *Diabetes* 62:1308–1319, 2013

Diabetic neuropathy is a common long-term complication of diabetes mellitus. According to epidemiological studies, at least 20% of patients with diabetes have a manifestation of diabetic polyneuropathy, and approximately one-half of these individuals have pain (1) that is difficult to treat and is known to be less susceptible to opioid analgesics. Only high doses of opioids, e.g., 400–600 mg tramadol (2) or 40–60 mg oxycodone (3), are reported to achieve a comparable therapeutic effect (i.e., number needed to treat, 3–5),

resulting in a high incidence of opioid-associated side effects such as sedation, cognitive dysfunction, constipation, nausea, and vomiting (4). Particularly in the elderly population, these side effects may have a great impact on quality of life (5).

In rodent models of streptozotocin (STZ)-induced diabetic neuropathy, the antinociceptive efficacy of opioids after their systemic (6), spinal (7,8), or supraspinal (8) administration is reduced relative to controls. Although various mechanisms for the loss of antinociceptive efficacy have been investigated mainly at the level of the spinal cord, the findings remain discordant (7,9,10). According to the American Diabetes Association, diabetic neuropathy defines the presence of symptoms or signs of peripheral nerve dysfunction in diabetes (1). On these peripheral sensory neurons, opioid receptors have been identified (11) that contribute to the antinociceptive effects of opioids (12). Consistently, the antinociceptive effects of systemic delta-opioid agonists were significantly attenuated in conditional knockout mice lacking delta-opioid receptors in peripheral sensory neurons (13). Moreover, μ-opioid receptor (MOR) expression, G-protein-coupling, and efficacy are enhanced during chronic inflammatory pain, resulting in increased opioid antinociception (11) and less tolerance, i.e., reduced antinociceptive efficacy on repeated administration (14). Interestingly, in animals with neuropathic pain attributable to a chronic constriction injury, axonal MORs at the constriction site are a potential target for local opioid application, resulting in potent analgesia (15).

In this study, we sought to investigate whether MOR density and functional coupling are impaired in peripheral sensory neurons as a consequence of diabetes, thereby decreasing opioid therapeutic efficacy. We hypothesized that the density of sensory neuron MOR is reduced because of enhanced Rab7-dependent lysosomal targeting of MOR in vivo. To test this hypothesis, we used the model of STZ-induced diabetes and used different strategies to reverse Rab7-dependent lysosomal targeting of sensory neuron MOR to restore their responsiveness to opioids.

RESEARCH DESIGN AND METHODS

Reagents. We used the following reagents: [³H]DAMGO (50 Ci/mmol); [³⁵S] GTPγS (1250 Ci/mmol); STZ; morphine; penicillin; fentanyl, naloxone; mouse monoclonal Rab7 antibody; high-performance liquid chromatography–purified Rab7 small interfering RNA (siRNA) sense (5′-UACUGGUUCAUGAGCGAU GUCUUUC-3′) and antisense (5′-GAAAGACAUCGCUCAUGAACCAGUA-3′); negative control siRNA (scrambled sequence; Sigma-Aldrich, Taufkirchen, Germany) (16); Max Suppressor In Vivo RNA-LANCEr II, a formulation that enables highly efficient delivery of siRNA into animals (Bio Scientific Corporation); scintillation fluid (Perkin Elmer Wallac, Turku, Finland); artificial cerebrospinal fluid; nerve growth factor (NGF) (R&D Systems, Minneapolis,

MN); rabbit polyclonal MOR antibody (Gramsch Laboratories, Schwabhausen, Germany); mouse monoclonal GAD 65 antibody (Millipore GmbH, Schwalbach/Ts, Germany); rabbit polyclonal insulin (total insulin) antibody (Cell Signaling Technology, Danvers, MA); guinea pig polyclonal calcitonin gene–related peptide antibody (Peninsula Laboratories); mouse monoclonal antibody to rat lysosome–associated membrane glycoprotein-1 (Santa Cruz Biotechnology); and chicken polyclonal PGP9.5 antibody (EnCor Biotechnology).

STZ-induced diabetes. Experiments were conducted in age-matched male Wistar rats in accordance with the science-based guidelines for laboratory animal care of the National Research Council (2003) and were approved by the local animal care committee. Rats received an intravenous injection of STZ at 45 mg/kg in 0.8 mL of citrate buffer (0.03 mol/L, pH 4.7). The age-matched control animals received an equal volume of citrate buffer alone. Diabetes was verified 3 days later by measuring blood hyperglycemia in the tail vein blood using a glucose strip Glucoflex (H&H DiabetesCare GmbH, Waiblingen, Germany).

Antinociceptive testing. Mechanical pain thresholds were assessed by a paw pressure algesiometer before (baseline) and after intraplantar injections of the opioid agonist fentanyl (0.5–1.25 μg/100 μL) as previously described (11,17). Paw pressure thresholds (PPT) were expressed as raw data in grams or as percent maximum possible effect according to the following equation: $(\text{PPT}_{postinjection} - \text{PPT}_{basal}) / (140_{cut\text{-}off} - \text{PPT}_{basal})$ to correct for differences in baseline and to set the data in relation to the maximal effect of control animals. Because of previous controversies, thermal testing was not performed despite growing literature of its potential importance (18).

Experimental groups. Animals were subdivided into six groups (n = 6–8 rats per group): control, diabetic (STZ-treated), diabetic rats receiving intrathecal Rab7 siRNA or negative control siRNA, and diabetic rats with intrathecal NGF or vehicle. Intrathecal catheters were implanted as previously reported (18). Rats received the following intrathecal treatments: for intrathecal β-NGF delivery, Alzet osmotic minipumps (200 μL; Alzet Corporation, Cupertino, CA) were filled with artificial cerebrospinal fluid and rat serum albumin (1 mg/1 mL) with or without 0.125 μg/1 μL NGF and connected to the intrathecal catheter to administer NGF or vehicle continuously at 1 μL/h over 7 days during the week 12 of STZ according to previous protocols (19). All tests were performed on day 8 after pump implantation. In vivo siRNA delivery was performed as follows: Rab7 siRNA and negative control siRNA were dissolved in Max Suppressor In Vivo RNA-LANCEr II to a final concentration of 2 μg/10 μL, which was administered as intrathecal boluses twice at the 1st and 3rd day of the 12th week of STZ-induced diabetes (20). RT-PCR of Rab7 mRNA and Western blot of Rab7 were performed at 6 and 24 h, respectively, after the last injection of siRNA. MOR immunohistochemistry in dorsal root ganglia (DRG) was examined 48 h after the last siRNA injection. Finally, behavioral tests and MOR immunohistochemistry in the skin were performed 6 days after initiation of siRNA treatment.

Radioligand binding assay. Membranes were obtained from the lumbar (L4–5) DRG as described previously (21,22). MOR-specific binding of [^{3}H]DAMGO was performed as described previously (22). Briefly, cell membranes (200–300 μg) were incubated in assay buffer with increasing doses of DAMGO (0.02–2 nmol/L at 65 Ci/mmol; Amersham Pharmacia Biotech, Buckinghamshire, England) in the absence or presence of 10 μmol/L naloxone. Membranes were incubated in a final volume of 1 mL for 1 h at 30°C in assay buffer. Filters were soaked in 0.1% (w/v) polyethyleneimine solution for 30 min before use. Bound and free ligands were separated by rapid filtration under vacuum through Whatman GF/B glass fiber filters. Bound radioactivity was determined by liquid scintillation spectrophotometry at 70% counting efficiency for [^{3}H] after overnight extraction of the filters in 3 mL scintillation fluid (EG&G Wallac, Turku, Finland). All experiments were performed in duplicate and performed three times. MOR [^{35}S]GTPγS binding assay in DRG membranes was performed as previously described (21). Various concentrations (0.05–2 nmol/L) of [^{35}S]GTPγS (1,250 Ci/mmol; New England Nuclear, Boston, MA) were incubated with 50 μm GDP in assay buffer for 2 h at 30°C. At each concentration of [^{35}S]GTPγS, basal binding was assessed in the presence of GDP and absence of DAMGO, whereas specific binding was determined in the presence of 10 μmol/L DAMGO. Basal (unstimulated) [^{35}S]GTPγS binding was subtracted from DAMGO-stimulated binding at each measurement to determine net DAMGO-stimulated [^{35}S]GTPγS binding. All experiments were performed in duplicate.

NGF fluorometric two-site enzyme-linked immunoassay. NGF concentrations in DRG of control animals, diabetic animals, and diabetic animals treated with intrathecal β-NGF were quantified to characterize a possible inverse relationship of NGF with Rab7 that has been shown in vitro previously (23). After thawing and weighing the wet-weight DRG, tissue was homogenized on ice in 700 μL of homogenization buffer and again was stored at −80° C until NGF was measured by a modified two-site enzyme-linked immunoassay for rat β-NGF, which was purchased from R&D Systems (Duo Set ELISA Development Kit) (24). Endogenous NGF content was calculated as picograms of NGF per milligram of wet-weight tissue.

Quantitative Taqman RT-PCR. Total RNA was extracted from L4–5 DRG using the RNeasy (Qiazol Lysis Reagent) Kit (Qiagen, Hilden, Germany). The following specific primers were used: for rat Rab7 mRNA upstream, 5′-TACAAAGCCACAATAGGAGCAGACTT-3′ and downstream, 5′-ATTGATGGCCTCCTTGGCACTGGTCT-3′ (accession no. AF286535) (25); for MOR mRNA upstream, 5′-TTACGGCCTGATGATCTTACGA-3′ and downstream, 5′-GGTGATCCTGCGCAGATTC-3′ (accession no. AY225403) (26); for 18S rRNA upstream, 5′-CGGCTACCACATCCAAGGAA-3′ and downstream 5′-GCTGGAATTACCGCGGCT-3′ (accession no. M11188.1) (27). Taqman quantitative RT-PCR was performed as described previously (26).

Western blot analysis. L4–5 DRG were solubilized according to Mousa et al. (26) to obtain total cell protein. For quantifying membrane-bound versus cytsolic (e.g., internalized) MOR, subcellular fractionation was performed as previously described (28). The protein distribution between membrane and cytosol fractions was assayed by Western blot analysis as previously described (26). The Western blot bands of MOR and Rab7 were quantified by Java Image processing and analysis software (ImageJ; open-source image software downloaded from the Internet) as described previously (18).

Immunohistochemistry. After perfusion of rats, pancreas, DRG, and skin were removed and further processed as described previously (11). The method of immunostaining DRG and skin has been described in detail elsewhere (11,18). Briefly, we stained every fourth section of DRG that was serially cut at 10 μm for each animal (n = 5) with respective antibodies. DRG neurons with a distinct nucleus were counted in five sections per animal to determine the total number of neurons per transverse section and the number and percentage of neurons immunoreactive for MOR (n = 5 rats). Consistent with the total MOR number in DRG, the total number of MOR neurons per area (38.4 mm^2) was counted in the skin (five tissue sections per animal) with the dermal–epidermal junction in the middle axis of the area. Immunostained PGP9.5-IR (immunoreactive) nerve fibers were counted at the dermal–epidermal junction of the skin as nerve fibers crossing or originating at the basement membrane excluding fiber branching. Five squares per each section were analyzed using a Zeiss microscope as described previously (29). For measurements of membrane-bound MOR immunoreactivity (outer ring) versus cytosolic enrichment in MOR-IR DRG neurons, representative images for DRG neurons from different treatment groups were taken. Measurements were conducted as previously described (30) using Java Image processing and analysis software. Briefly, the outer borders of neuronal somata for a minimum of 100 neurons from 5 rats of each group were manually traced with line thickness set to 3 μm to measure membrane-associated immunoreactivity. The respective encircled areas served to measure intracellular immunoreactivity (cytosolic enrichment). The ratio of the fluorescence intensity of the outer borders (plasma membrane) to that of cytosolic enrichment (intracellular immunoreactivity) was used to assess the degree of membrane versus cytosolic enrichment. Data were expressed as means ± SEM.

Statistics. All statistics were performed using the Sigma Stat 2.03 (SPSS Science, Chicago, IL) software. Data were reported as means ± SD or SEM and were compared by one-way or two-way ANOVA if the normality test was passed (Kolmogorov-Smirnov test). Otherwise, the Kruskal-Wallis ANOVA on ranks was used. Post hoc multiple pair-wise comparisons were performed by the Tukey test or Student-Newman-Keuls test. Data of two groups were compared by the two-tailed Student t test or Mann-Whitney U test. For the analysis of behavioral dose-dependent effects, a linear regression ANOVA was applied. $P < 0.05$ was considered significant.

RESULTS

Elevated blood glucose, reduced weight gain, and mechanical hyperalgesia in rats with STZ-induced diabetes. Rats receiving intravenous 45 mg/kg STZ showed an apparent loss in insulin-producing GAD65-IR endocrine cells of the pancreas (Fig. 1A), concomitant with significantly increased blood glucose ($P < 0.05$; Fig. 1B), reduced weight gain ($P < 0.05$; Fig. 1B), and the development of mechanical hyperalgesia (decreased PPT) ($P < 0.05$; Fig. 2A); however, there was no difference in the number of PGP9.5-IR nerve fibers per millimeter at the dermal–epidermal junction of the skin (Fig. 1D and E).

Loss of opioid antinociceptive efficacy in diabetic rats. Intraplantar injection of low, systemically ineffective doses of fentanyl to control rats significantly increased PPT on the ipsilateral but not contralateral paw ($P < 0.05$; Fig. 2A and D), which was even more pronounced in
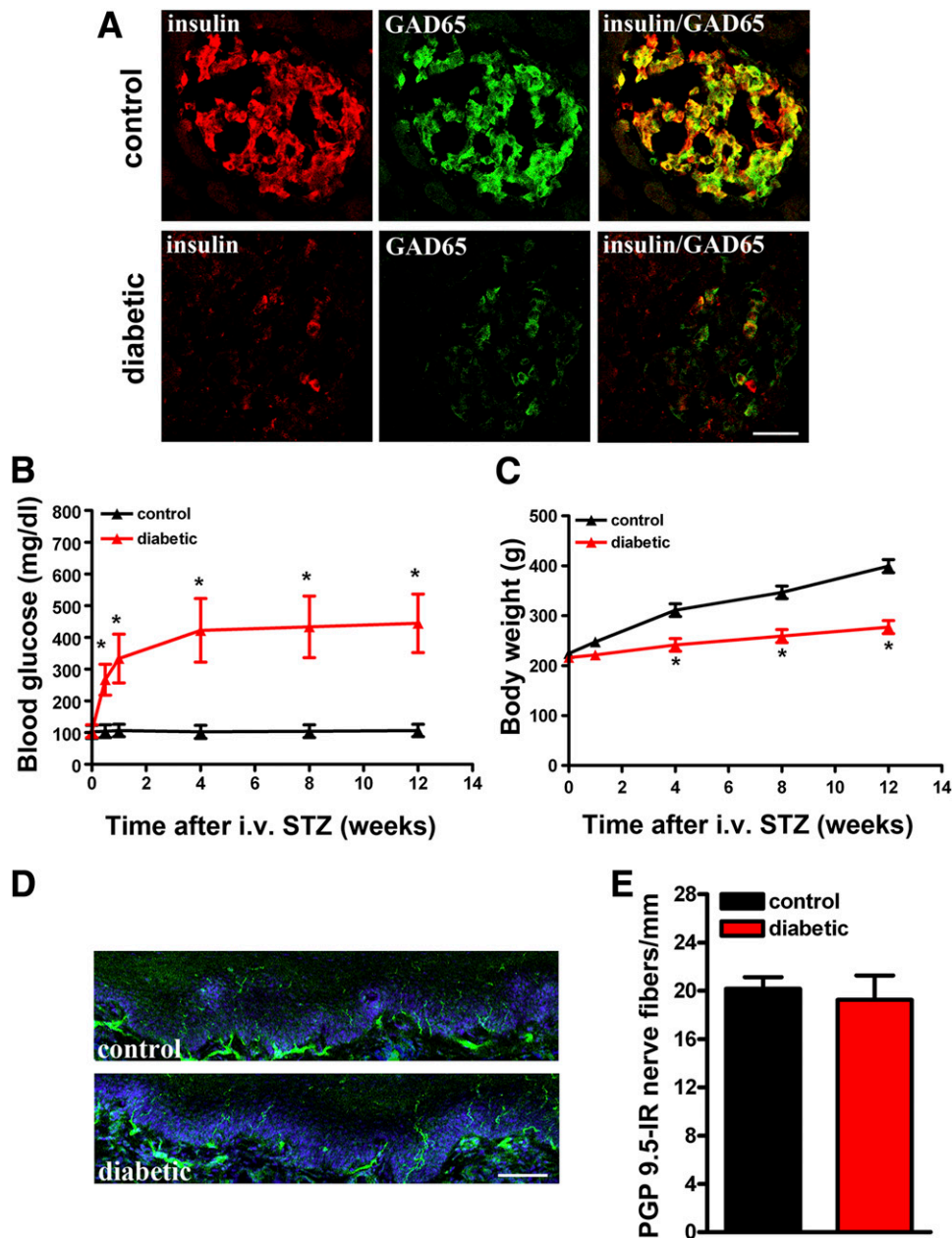
FIG. 1. Pathophysiological changes in rats with STZ-induced (45 mg/kg intravenous) diabetes. *A*: Representative double-immunofluorescence images showing markedly reduced coexpression of insulin (*red fluorescence*) and GAD65 (*green fluorescence*) in pancreatic β-cells of STZ-induced diabetic compared with control rats. Bar = 40 μm. *B*: After the intravenous injection of STZ (*red, n = 18*), blood glucose levels significantly increased up to 12 weeks compared with vehicle-treated rats (*black, n = 18*; *$P < 0.05$, two-way repeated measures [RM]-ANOVA, Tukey test). *C*: During the same time period the gain in body weight was significantly less in STZ (*red, n = 18*) vs. vehicle-treated rats (*black, n = 18*; *$P < 0.05$, two-way RM-ANOVA, Tukey test). Bar = 50 μm. *D*: Immunofluorescence images of PGP9.5-IR nerve fibers in control rats and rats treated with intravenous 45 mg/kg STZ. *E*: The number of nerve fibers crossing or originating at the dermal–epidermal junction was not different between both groups. All data are shown as means ± SD. (A high-quality color representation of this figure is available in the online issue.)

animals with CFA hindpaw inflammation ($P < 0.05$; Fig. 2*A* and *C*). In contrast, STZ-induced diabetes significantly reduced fentanyl-induced PPT elevations consistent with a loss in opioid antinociception ($P < 0.05$; Fig. 2*A* and *C*). The antinociception of intraplantar fentanyl was antagonized by increasing doses of the intraplantar opioid antagonist naloxone, confirming an opioid receptor–specific effect ($P < 0.05$; Fig. 2*B*). Dose-dependent antinociception of intraplantar fentanyl in diabetic animals was approximately two-fold or three-fold lower than in control or CFA-treated rats, respectively ($P < 0.05$; Fig. 2*C*).

Loss of MOR in DRG sensory neurons, axons, and peripheral nerve terminals. Confocal immunofluorescence showed colocalization of all MOR-IR DRG neurons with calcitonin gene–related peptide in diabetic and control rats (Fig. 3*A*). The percentage of MOR-IR per total cells in DRG was significantly reduced in diabetic compared with control animals ($P < 0.05$; Fig. 3*B*). Consistently, the integrated optical density of MOR-specific bands was significantly lower in diabetic rats compared with controls ($P < 0.05$; Fig. 3*C* and *D*). This loss was not attributable to reduced MOR gene transcription, because
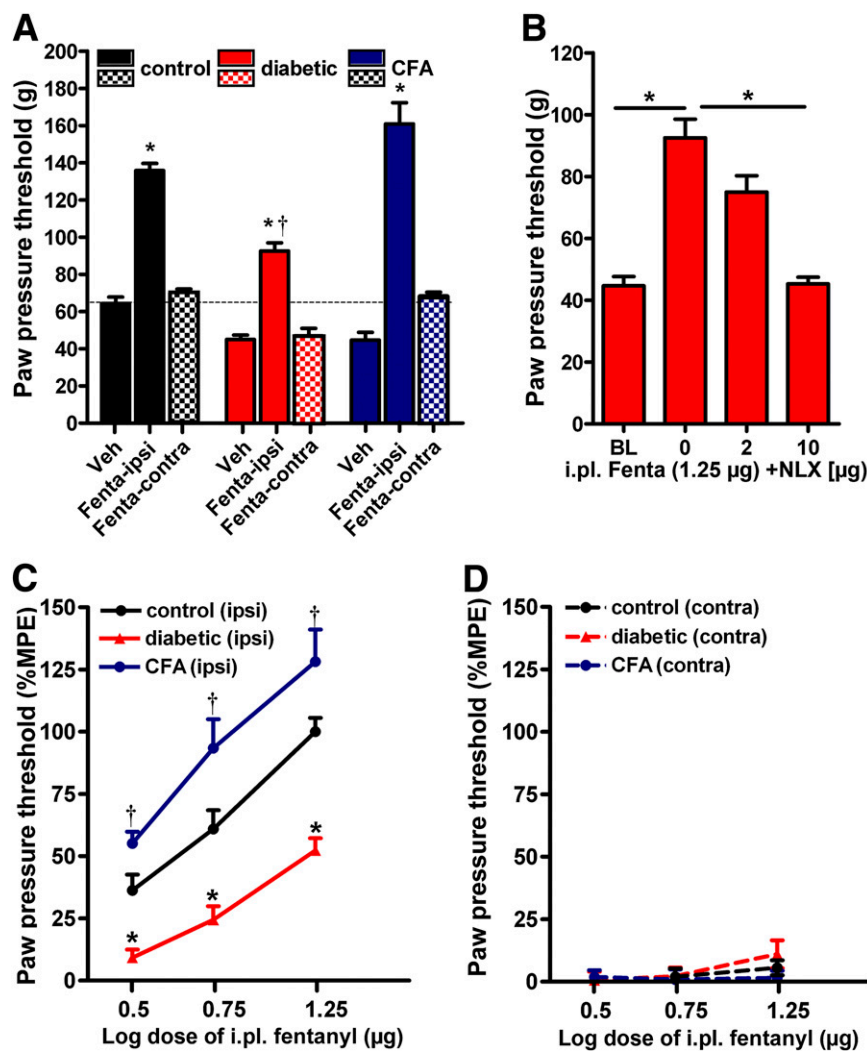
FIG. 2. Loss of sensory neuron opioid efficacy in diabetic rats. *A*: Increases in PPT after intraplantar fentanyl (Fenta) (1.25 μg), but not vehicle, were significantly smaller in diabetic compared with inflamed and control rats. These PPT elevations were not observed on the contralateral side excluding a systemic effect. *Significant differences compared with vehicle, †significant differences compared with control ($n = 6$; $P < 0.05$, one-way ANOVA, Tukey test). *B*: Compared with baseline, intraplantar fentanyl resulted in PPT elevations of diabetic animals that were dose-dependently reversed by intraplantar naloxone ($P < 0.05$, ANOVA on ranks, Student-Newman-Keuls tests). *C*: Dose–response curves of intraplantar (i.pl.) fentanyl showed that PPT elevations were significantly reduced in diabetic compared with control and rats after 4 days. Complete Freund adjuvant (CFA)–induced hind paw inflammation, reflecting impaired antinociception ($n = 6$; $P < 0.05$, two-way ANOVA, Tukey test). PPT values are given percent maximum possible effect (MPE) according to the equation: $(PPT_{postinjection} - PPT_{basal}) / (140_{cut-off} - PPT_{basal})$ to offset baseline differences. *D*: Dose–response curves on the contralateral side did not show significant PPT elevations. All data are shown as means ± SEM. (A high-quality color representation of this figure is available in the online issue.)

MOR mRNA levels did not differ between diabetic and control animals ($P < 0.05$; Fig. 3*E*). Consequently, the number of MOR-IR nerve fibers at the dermal–epidermal junction in diabetic animals was significantly decreased ($P < 0.05$; Fig. 4*A* and *B*).

Enhanced MOR targeting to lysosomes in DRG sensory neurons. Using fluorescence microscopy, MOR were localized predominantly to the plasma membrane of control DRG neurons with almost no evidence for a colocalization with Lamp-I or Rab7 (Fig. 5*A*). In contrast, in DRG of diabetic rats, MOR exhibited extensive colocalization with Rab7 in Lamp-I-IR perinuclear lysosome compartments. Quantitative analysis revealed a significantly decreased membrane-to-cytosol ratio of MOR within DRG neurons of diabetic animals compared with controls ($P < 0.05$; Fig. 5*B*). In support, DRG subfractionation studies revealed that the majority of MOR protein was confined to the cytosol and not to the membrane fraction in diabetic compared with control animals ($P < 0.05$; Fig. 5*C* and *D*). In addition, the maximal number of membrane MOR binding sites was significantly decreased in DRG of diabetic rats. Scatchard analysis revealed a Bmax value of 28 ± 4.3 fmol/mg protein for the DRG membranes of control and 14 ± 1.3 fmol/mg protein for diabetic animals ($P < 0.05$; Fig. 5*E*). Consequently, DAMGO-induced [^{35}S]GTPγS binding was significantly reduced in the DRG of diabetic relative to control rats ($P < 0.05$; Fig. 5*F*).

Reversal of MOR lysosomal targeting by silencing enhanced Rab7 expression. Both quantitative RT-PCR and Western blot analysis in DRG neurons of diabetic rats showed a significant increase of Rab7, but not of Rab4, relative to controls ($P < 0.05$; Fig. 6*A*–*D*). A Rab7 gene silencing approach, in which diabetic rats received intrathecal Rab7 siRNA, caused a significant reduction of Rab7 mRNA and protein in DRG neurons but not of Rab4 mRNA, internal reference RNA, and protein (18S RNA and
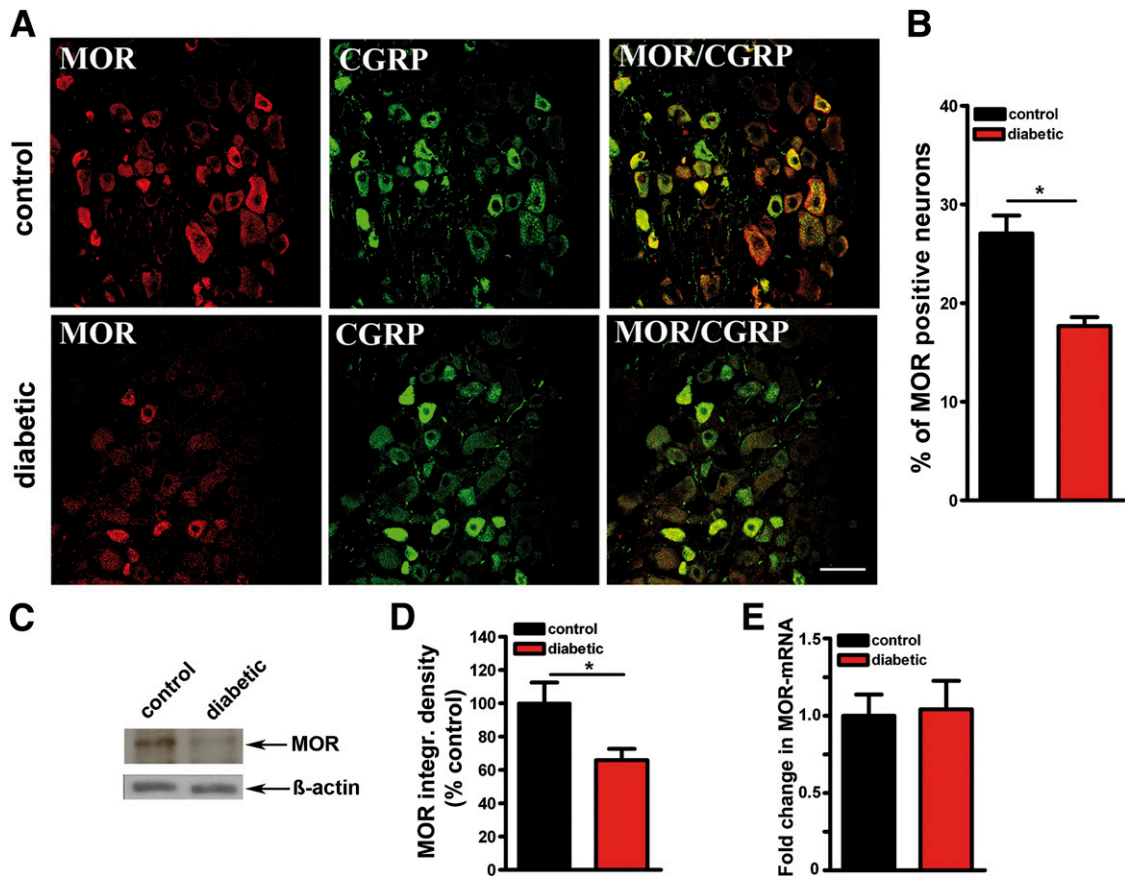
FIG. 3. Loss of sensory neuron MOR and enhanced MOR targeting to lysosomes in DRG neurons of diabetic rats. *A*: Double-immunofluorescence images represent colocalization of MOR (*red fluorescence*) with the sensory neuron marker calcitonin gene–related peptide (CGRP, *green fluorescence*) in DRG sections of control and diabetic rats. Bar = 40 μm. *B*: The number of MOR-IR neurons was markedly reduced in diabetic rats compared with controls ($n = 5$; *$P < 0.05$, Student t test). *C*: Western blot analysis of DRG from diabetic and control animals revealed a 55-kDa band specific for MOR and a 42-kDa band specific for β-actin. *D*: Densitometric image analysis (National Institutes of Health ImageJ software) of the respective protein bands showed that the density of the MOR protein band in DRG of diabetic rats was markedly reduced compared with control rats ($n = 6$; *$P < 0.05$, Student t test). *E*: Quantification of MOR mRNA in DRG neurons of diabetic and control rats using Taqman quantitative RT-PCR shows the MOR mRNA was not significantly different from DRG neurons of diabetic vs. control rats ($n = 9$; *$P > 0.05$, Student t test). All data are shown as means ± SEM. (A high-quality color representation of this figure is available in the online issue.)

β-actin protein) ($P < 0.05$; Fig. 6A–D). This treatment prevented the entry of MOR-IR vesicles into the lysosomal degradation pathway and MORs were again abundantly relocated to the sensory neuron plasma membrane ($P <$ 0.05; Fig. 6C–F). The reduced membrane-to-cytosol ratio ($P < 0.05$; Fig. 6E and F) and optical density of MORs ($P <$ 0.05; Fig. 7A–C) in DRG of diabetic animals were significantly reversed by intrathecal Rab7 siRNA but not by
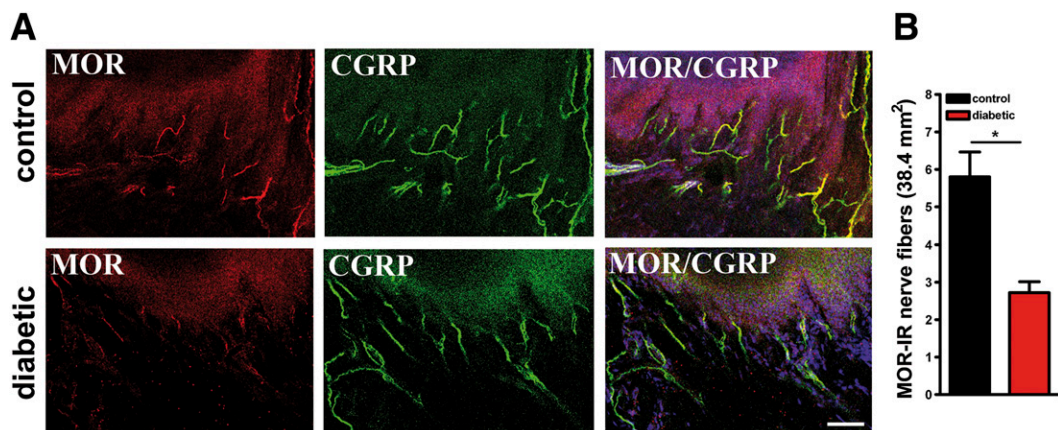

FIG. 4. *A*: Immunofluorescence images represent colocalization of MOR (*red fluorescence*) with sensory neuronal marker calcitonin gene–related peptide (CGRP, *green fluorescence*) on nerve endings within subcutaneous paw tissue of control and diabetic rats. Note, MOR-IR nerve fibers were reduced at the dermal–epidermal junction of the innervated skin of diabetic compared with control rats. Bar = 20 μm. *B*: Quantitative analysis showed that the number of MOR-IR nerve fibers was significantly reduced in diabetic compared with control rats ($n = 5$; *$P < 0.05$, Student t test). All data are shown as means ± SEM. (A high-quality color representation of this figure is available in the online issue.)
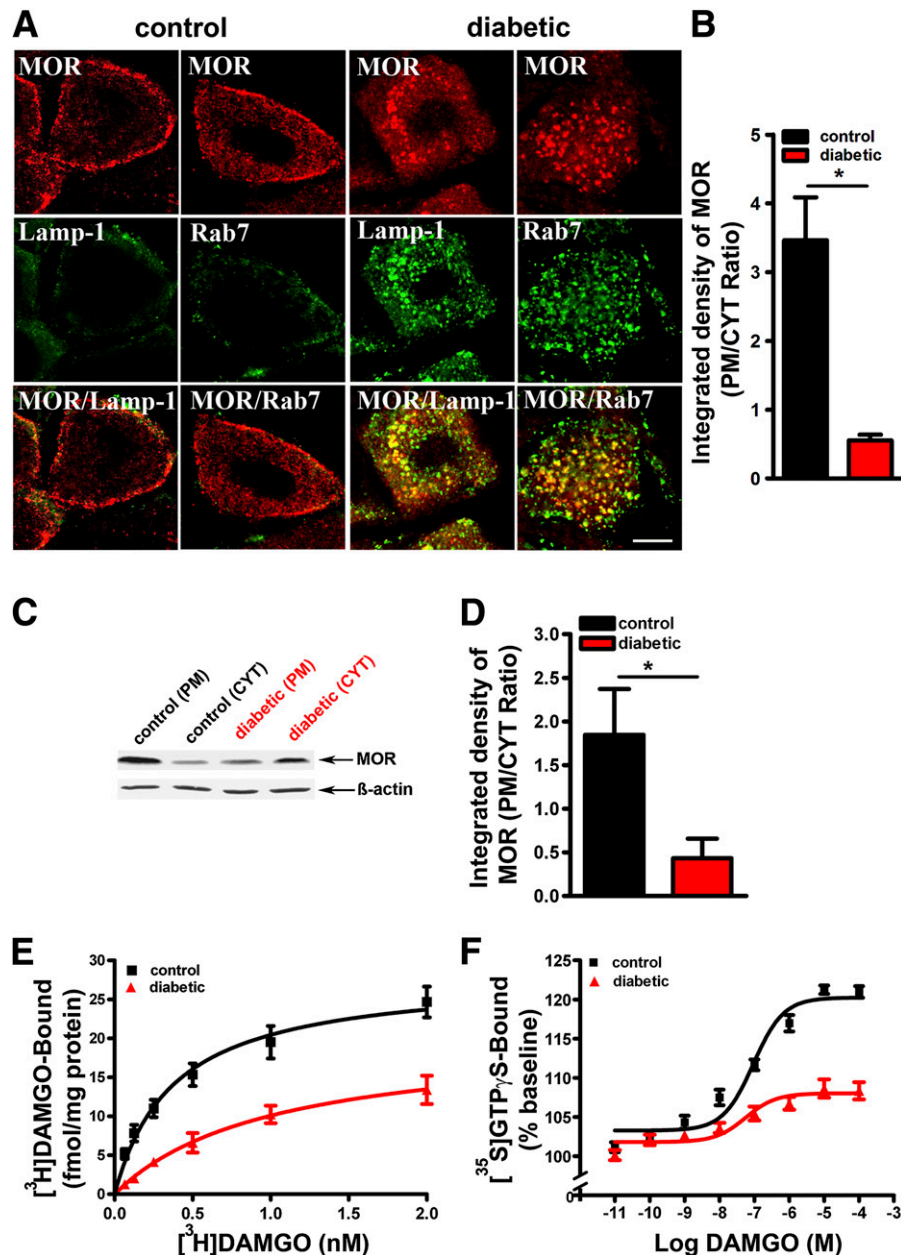
FIG. 5. Enhanced MOR lysosomal targeting occurs in parallel with a decrease in membrane-bound MOR and a loss in MOR G-protein-coupling in DRG of diabetic rats. *A*: Immunofluorescence images present colocalization of MOR (*red fluorescence*) with Rab7 or lysosomal marker lysosome–associated membrane glycoprotein-1 (LAMP-1; *green fluorescence*) in DRG. In control animals, MOR localized mainly to the cell surface of DRG neurons, whereas in diabetic rats MOR colocalized with Rab7 and Lamp1 (*yellow*) predominantly in the perinuclear lysosome compartment of the cytoplasm. Bar = 10 μm. *B*: Quantitative analysis of the relative MOR distribution in the plasma membrane (PM) vs. cytoplasm (CYT) showed that the PM/CYT ratio of MOR was significantly reduced in DRG of diabetic compared with control rats ($P < 0.05$, Student t test). *C* and *D*: Quantitative Western blot analysis of MOR in plasma membrane vs. cytosolic fractions of DRG neurons showed that the PM/CYT ratio of the integrated optical density of MOR was significantly reduced in diabetic compared with control rats, reflecting a reduction of MOR in the neuronal plasma membrane of diabetic rats ($n = 4$; *$P < 0.05$, Student t test). *E*: Saturation binding of [^{3}H]DAMGO in membrane fractions of DRG from diabetic compared with control rats ($n = 6$). The maximal number of MOR binding sites in membrane fractions of diabetic rats was significantly reduced compared with controls ($P < 0.05$, two-way ANOVA). *F*: The stimulated [^{35}S]GTPγS binding to MOR of DRG membranes showing a significant reduction in the maximum efficacy of diabetic compared with control rats ($n = 6$; *$P < 0.05$, two-way ANOVA, Tukey test). All data are shown as means ± SEM. (A high-quality color representation of this figure is available in the online issue.)

negative control siRNA. Consequently, the reduced number of MOR-IR nerve fibers at the dermal–epidermal junction of the innervated skin recovered after intrathecal Rab7 siRNA application at days 1 and 3 of week 12 of STZ-induced diabetes ($P < 0.05$; Fig. 7*D* and *E*).

Reversing NGF deprivation normalizes Rab7 expression and restores sensory neuron MOR density and coupling in diabetic rats. NGF content was significantly reduced in

the DRG of diabetic rats relative to controls ($P < 0.05$; Fig. 8*A*). Intrathecal infusion of NGF over the course of 7 days restored NGF concentration in diabetic rats to that of controls. In line with a previous report that NGF deprivation enhances Rab7 expression and activation (30), enhanced Rab7 protein expression in diabetic rats was significantly reversed by intrathecal NGF treatment ($P < 0.05$; Fig. 8*B*). Furthermore, when Rab7 expression in DRG of diabetic rats
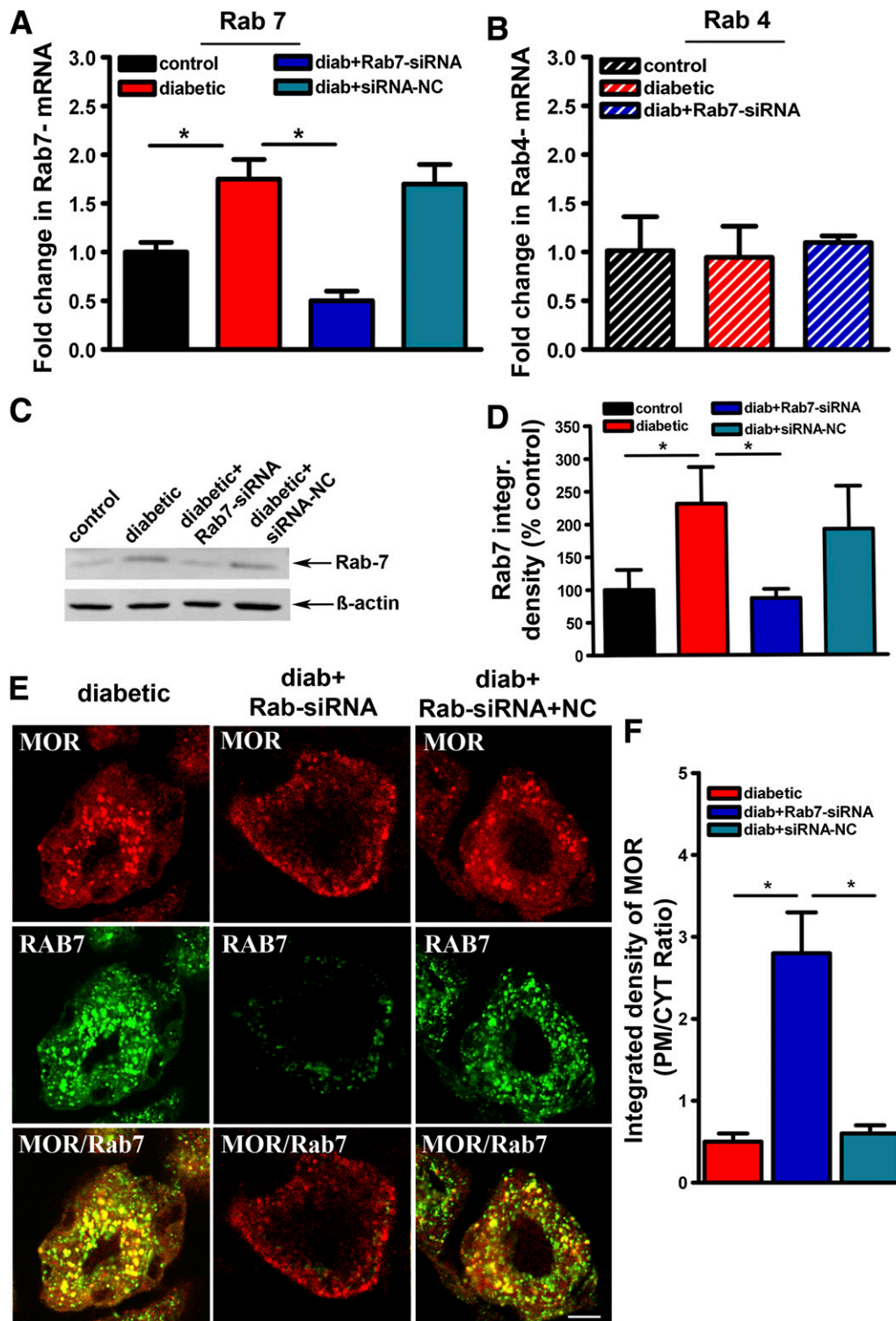
FIG. 6. Reversal of MOR lysosomal targeting by silencing enhanced Rab7 expression. *A*: Quantitative analysis of Taqman RT-PCR of Rab7 mRNA revealed a significant increase in Rab7 mRNA in diabetic rats that was abolished by intrathecal Rab7 siRNA, but not by a negative control siRNA treatment, on days 1 and 3 of week 12 of STZ-induced diabetes. *Significant differences compared with control nondiabetic as well as diabetic rats treated with intrathecal siRNA rab7 ($n = 6$; $P < 0.05$, one-way ANOVA, Dunn test). *B*: Quantitative analysis of Taqman RT-PCR of Rab4 mRNA revealed no change in Rab4 mRNA in diabetic rats with or without intrathecal Rab7 siRNA compared with vehicle ($n = 6$; $P > 0.05$, one-way ANOVA, Dunn test). *C*: Similar changes in the Rab7 protein band (24 kDa) were identified by Western blot analysis of DRG from diabetic rats treated with intrathecal Rab7 siRNA. *D*: Densitometric image analysis of Rab7 protein bands showed that the integrated density was significantly increased in DRG of diabetic rats; however, it was significantly reduced in diabetic rats treated with intrathecal Rab7 siRNA but not with negative control siRNA ($n = 4$; $P < 0.05$, ANOVA on ranks, Dunn test). *E*: Representative laser-scanning confocal micrographs showed a redistribution of perinuclear MOR (*red fluorescence*) in DRG neurons of diabetic animals to the plasma membrane of neuronal DRG after intrathecal Rab7 siRNA but not with negative control siRNA treatment. Bar = 10 μm. *F*: Quantitative analysis of the plasma membrane/cytoplasm (PM/CYT) ratio of MOR showed that the integrated optical density of MOR is significantly increased in DRG of diabetic rats treated with intrathecal Rab7 siRNA but not with negative control siRNA ($P < 0.05$, one-way ANOVA, Dunn test). All data are shown as means ± SEM. (A high-quality color representation of this figure is available in the online issue.)
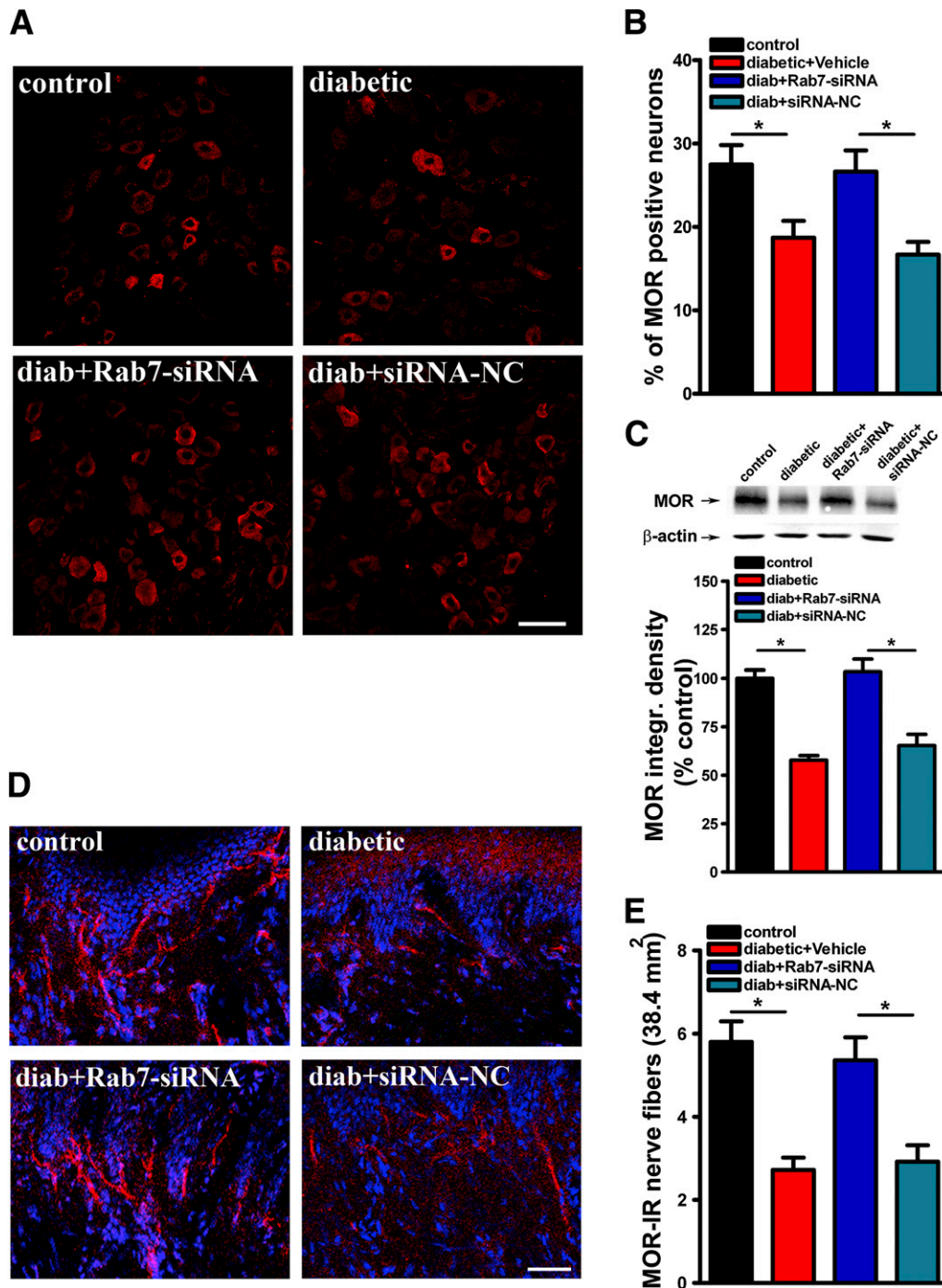
FIG. 7. Silencing enhanced Rab7 expression in diabetic rats restores MOR in sensory neurons. *A*: Immunofluorescence images represent MOR-IR DRG neurons from control, diabetic, and diabetic rats treated with Rab7 siRNA or with negative control siRNA. Bar = 40 μm. *B*: The reduced number of MOR-IR DRG neurons in diabetic rats was significantly reversed after intrathecal Rab7 siRNA, but not negative control siRNA, on days 1 and 3 of week 12 of STZ-induced diabetes ($n = 5$; *$P < 0.05$, ANOVA on Ranks, Tukey test). *C*: Similarly in Western blot, the reduced intensity of MOR protein bands in DRG neurons was reversed by intrathecal Rab7 siRNA. Densitometric image analysis showed that the reduced integrated density of MOR protein bands in DRG of diabetic rats ($n = 4$) was reversed by intrathecal Rab7 siRNA (*$P < 0.05$, ANOVA on Ranks, Tukey test). *D*: Immunofluorescence images showing MOR-IR nerve fibers at the dermal–epidermal junction of the innervated skin of control rats, diabetic rats, and diabetic rats treated with intrathecal Rab7 siRNA or negative control siRNA. Bar = 40 μm. *E*: The significantly reduced number of MOR-IR nerve fibers was reversed by intrathecal Rab7 siRNA, but not by negative control siRNA ($n = 5$; *$P < 0.05$, ANOVA on Ranks, Tukey test). All data are shown as means ± SEM. (A high-quality color representation of this figure is available in the online issue.)

was restored to that of control animals, the loss of MOR receptor protein in DRG of diabetic rats was significantly reversed (Fig. 8*C*). In addition, after intrathecal NGF treatment, the impairment of MOR G-protein-coupling ([^{35}S] GTPγS binding) was abolished ($P < 0.05$; Fig. 8*D*).

Inhibition of MOR lysosomal targeting restores MOR-mediated analgesia in diabetic rats. To determine whether these interventions enhance the antinociceptive effects of the MOR agonist fentanyl in diabetic rats, we assessed the effects of fentanyl on PPT in animals that
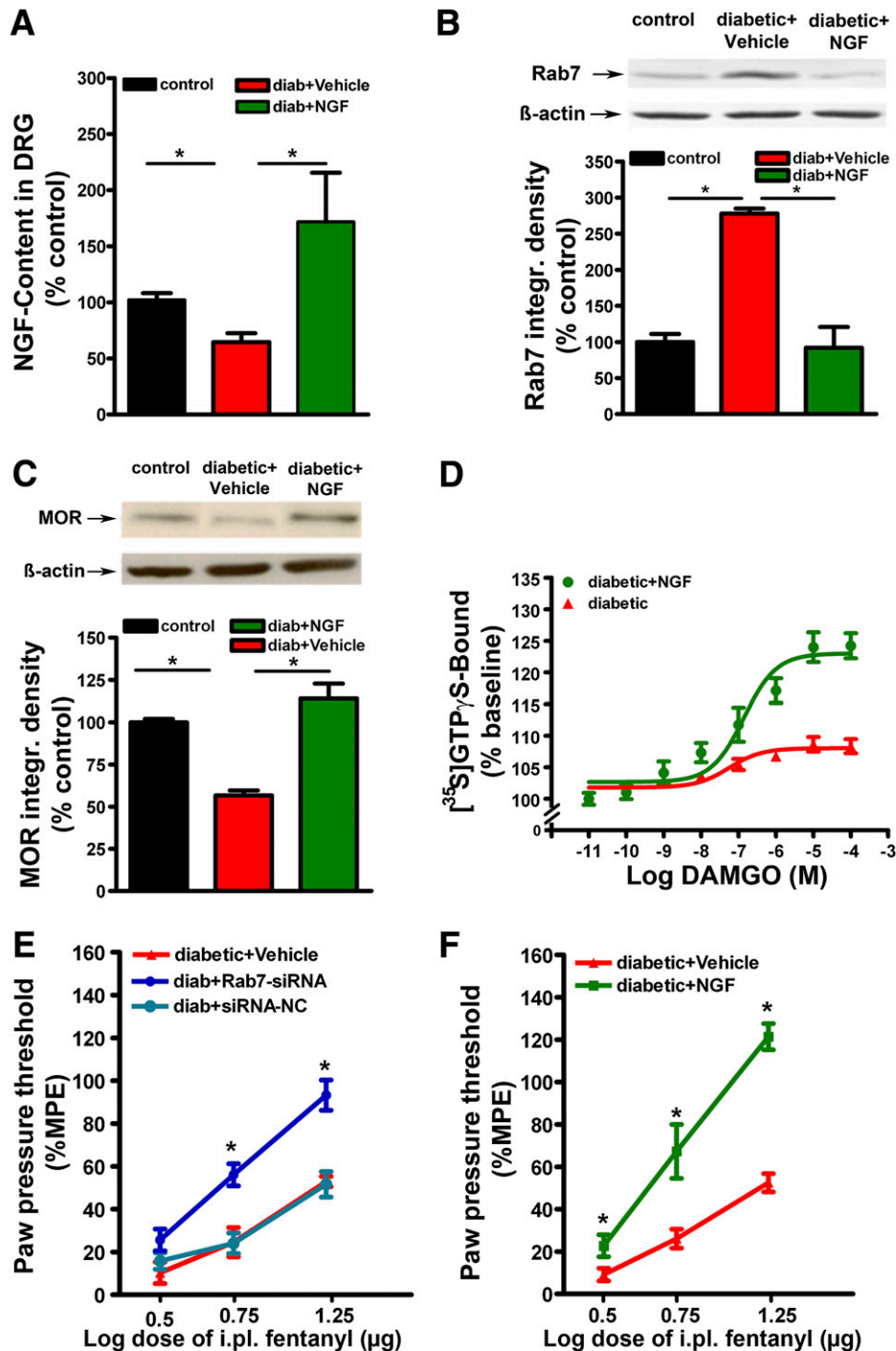
FIG. 8. Normalizing Rab7 expression in DRG by intrathecal NGF over 7 days rescued sensory neuron MOR number and efficacy in diabetic rats. *A*: Determination of NGF content by a fluorometric enzyme–linked immunoassay in DRG of control, diabetic, and diabetic rats treated with intrathecal NGF. Note, NGF content in DRG of diabetic rats was reduced by ~40% compared with control, which can be reversed after intrathecal NGF treatment ($n = 4$; *$P < 0.05$, ANOVA on ranks, Student-Newman-Keuls test). *B*: In Western blots, increased density of Rab7 in DRG of diabetic compared with control rats was completely reversed by intrathecal NGF treatment ($n = 4$; *$P < 0.05$, ANOVA on ranks, Tukey test). *C*: Inversely related to this, the reduced density of MOR protein bands in DRG of diabetic animals returned to control values after intrathecal NGF treatment ($n = 4$; *$P < 0.05$, ANOVA on ranks, Tukey test). *D*: The reduced DAMGO-stimulated [^{35}S]GTPγS binding to MOR of DRG membranes from diabetic rats was reversed by intrathecal NGF treatment ($n = 8$; *$P < 0.05$, two-way ANOVA, Tukey test). *E*: The significantly reduced PPT after intraplantar fentanyl in diabetic rats were reversed by intrathecal Rab7 siRNA, but not by negative control siRNA ($n = 6$; *$P < 0.05$, two-way ANOVA, Tukey test). PPT values were given as means ± SEM of percent maximum possible effect. *F*: Similarly, the significantly reduced PPT after intraplantar (i.pl.) fentanyl in diabetic rats was prevented by intrathecal NGF ($n = 6$; *$P < 0.05$, two-way ANOVA, Tukey test). PPT values are given as means ± SEM of percent maximum possible effect. (A high-quality color representation of this figure is available in the online issue.)

received intrathecal Rab7 siRNA on days 1 and 3 or intrathecal NGF over the course of 7 days of week 12 of STZ-induced diabetes (Fig. 8*E* and *F*). Consistent with the functional opioid recovery, the impaired fentanyl-induced

antinociception in diabetic animals was restored after both intrathecal Rab7 siRNA and NGF ($P < 0.05$; Fig. 8*E* and *F*), similar to the blockade of MOR lysosomal targeting and degradation in peripheral sensory neurons of diabetic rats.

DISCUSSION

This study demonstrates in the model of STZ-induced painful diabetic neuropathy that the impaired antinociceptive effects of opioids are associated with a loss in MOR number and G-protein-coupling of peripheral sensory neurons. Under normal conditions, MORs are localized primarily on the cell membrane of peripheral sensory neurons. In contrast, in diabetic neuropathy, a loss of MOR is associated with enhanced Rab7 expression and a colocalization of MOR with Rab7 in LampI-positive perinuclear lysosome compartments. Different strategies such as Rab7 siRNA knockdown and intrathecal NGF treatment resulted in the normalization of Rab7 expression and the subsequent reversal of Rab7-dependent lysosomal targeting, which finally restored MOR density on the cell membrane of sensory neurons and rescued opioid responsiveness toward better pain control.

It is well established in experimental (11) and clinical (12) studies that inflammatory pain leads to the upregulation of MOR on peripheral sensory neurons and consequently potentiates the peripheral antinociception elicited by local opioids (12,18,21). In contrast, in diabetic animals, the antinociceptive effects of intraplantar fentanyl were greatly reduced, with the extent of this reduction being significantly larger than the differences in baseline pain thresholds. Because peripheral opioid antinociception is dependent on peripheral sensory neuron MOR number, coupling, and efficacy (11,22), we hypothesized that changes in sensory neuron MOR of STZ-induced diabetic rats are responsible for this loss in opioid responsiveness. The number of small MOR-IR DRG neurons, which coexpressed the sensory neuron marker calcitonin gene–related peptide, as well as the total amount of MOR protein were significantly reduced, a fact that was not described in previous studies (6–8,31). In addition, the peripheral nerve terminals of these neurons showed a reduction in MOR immunoreactivity at the dermal–epidermal junction without changes in the number of PGP9.5 nerve endings. Consistently, previous studies have shown that even long-term STZ-induced diabetes is associated with a relative preservation of sensory neuron populations (32).

To follow-up the fate of the MOR, we performed immunfluorescence confocal microscopy in DRG sections of diabetic and control rats in which MOR immunoreactivity was highly concentrated in the plasma membranes of neurons from control DRG, whereas they were highly localized in LampI-positive perinuclear lysosome compartments of diabetic animals (33,40). Intracellular receptor trafficking is important for the function of G-protein-coupled receptors (34). They can be internalized by agonist-induced endocytosis (34), heterologous protein kinase–mediated endocytosis (35), or by constitutive endocytosis (36), resulting in their delivery to the intracytoplasmatic compartment of early endosomes. There, they can be recycled back to the plasma membrane in a fully sensitized state (15) or delivered to lysosomes for degradation (34), dependent on small monomeric Rab GTPases such as Rab7 GTP-binding protein (37). Here, the number of MOR binding sites in the plasma membrane as well as the maximal efficacy in MOR G-protein-coupling was significantly reduced in DRG of diabetic rats, which contributes to a loss in agonist efficacy (38).

Apparently, peripheral sensory neuron MORs in diabetic animals seem to enter the lysosomal pathway, undergo subsequent degradation, and result in the loss of opioid responsiveness. Rab7 has been considered in mammalian cells as a key regulatory protein for the intracellular vesicle traffic toward perinuclear lysosome compartments (39,40). Consistently, Rab7 mRNA and protein levels were highly upregulated in diabetic animals. Therefore, we applied intrathecal delivery of Rab7 siRNA to silence the endogenous expression of Rab7 in peripheral sensory neurons (20,41). As a result, intrathecal Rab7 siRNA, but not scrambled RNA, led to a dramatic reduction of both Rab7 mRNA and protein. Importantly, other members of the Rab GTPases family, such as Rab4, were not affected. Rab7 siRNA treatment also abolished the localization of MOR to Rab7-IR perinuclear lysosomal compartments and reversed the number of MOR-IR sensory neurons. Similarly, Balut et al. (41) showed that in vitro siRNA-mediated knockdown of Rab7 resulted in a significant inhibition of the plasma membrane–associated KCa3.1 channel degradation rate. To the best of our knowledge, these results represent the first in vivo report on the peripheral sensory neuron MOR downregulation through the Rab7-mediated lysosomal degradation pathway during diabetic neuropathy. Until now, agonist-induced downregulation of G-protein-coupled receptors via the lysosomal pathway has been reported mainly in vitro (34,42).

The maintenance of nociceptive sensory neurons depends on NGF, a neurotrophic factor with the ability to resist apoptosis and to foster regenerative capacity (43). NGF is expressed in peripheral tissues such as the skin, binds to the high-affinity receptor trkA of petidergic peripheral sensory nerve terminals, is retrograde-transported to the DRG, and regulates the expression of ion channels and receptors of these neurons (43). Recently, we have demonstrated that >80% of sensory neuron MOR colocalize with trkA in the NGF-dependent subpopulation of small DRG neurons (11). In diabetic rats, peripheral sensory neurons suffer from a persistent deficit in NGF concentration (24,44,45). Moreover, growth factor deprivation leads to the upregulation of Rab7 expression (23). In this study, we observed a significant reduction in NGF concentrations of sensory DRG neurons from diabetic rats concomitant with a high increase in Rab7 mRNA and protein levels, suggesting a causal relationship. Intrathecal NGF treatment of diabetic animals clearly reduced the enhanced Rab7 mRNA and protein. Subsequently, the total number of MOR-IR sensory neurons, the relative number of membrane spanning MOR in DRG, and the MOR on peripheral sensory nerve endings returned back to baseline values, supporting the interdependence between NGF and Rab7 (23). Finally, behavioral experiments showed that the antinociceptive effects of opioids were clearly improved in diabetic animals by the normalization of Rab7 expression as well as by intrathecal NGF treatment.

These results provide novel insights into the loss of the MOR number, functional coupling, and antinociceptive efficacy of peripheral sensory neurons suffering from diabetic neuropathy. Moreover, they show for the first time in vivo that enhanced Rab7-dependent lysosomal targeting and degradation of MOR during diabetic neuropathy contribute to the downregulation of peripheral sensory neuron MOR. This may explain why diabetic patients sometimes do not respond to increasing doses of opioids at all, except with an increase in the occurrence of serious side effects. Importantly, the blockade of the enhanced Rab7 expression in diabetes, e.g., by substitution of NGF, prevented MOR targeting to lysosomes, restored MOR density in the cell membrane of sensory neurons, and rescued opioid

responsiveness toward better pain relief. This is in contrast to other pathological pain states such as inflammatory pain in which the sensory neuron MORs and antinociception are enhanced and provides intriguing evidence that regulation of opioid responsiveness varies as a function of pain pathogenesis. After all, these findings may caution the unreflected use of the anti-NGF monoclonal antibody (46), which has been developed recently for the treatment of chronic pain.

REFERENCES

1. Boulton AJM, Vinik AI, Arezzo JC, Bril V, Feldman EL, Freeman R, Malik RA, Maser RE, Sosenko JM, Ziegeler D. Diabetic neuropathies: A statement by the American Diabetes Association. Diabetes Care 2004;28:956–962
2. Harati Y, Gooch C, Swenson M, et al. Maintenance of the long-term effectiveness of tramadol in treatment of the pain of diabetic neuropathy. J Diabetes Complications 2000;14:65–70
3. Watson CP, Moulin D, Watt-Watson J, Gordon A, Eisenhoffer J. Controlled-release oxycodone relieves neuropathic pain: a randomized controlled trial in painful diabetic neuropathy. Pain 2003;105:71–78
4. Dworkin RH, O'Connor AB, Audette J, et al. Recommendations for the pharmacological management of neuropathic pain: an overview and literature update. Mayo Clin Proc 2010;85(Suppl):S3–S14
5. Annemans L. Pharmacoeconomic impact of adverse events of long-term opioid treatment for the management of persistent pain. Clin Drug Investig 2011;31:73–86
6. Courteix C, Bourget P, Caussade F, et al. Is the reduced efficacy of morphine in diabetic rats caused by alterations of opiate receptors or of morphine pharmacokinetics? J Pharmacol Exp Ther 1998;285:63–70
7. Chen SR, Pan HL. Antinociceptive effect of morphine, but not mu opioid receptor number, is attenuated in the spinal cord of diabetic rats. Anesthesiology 2003;99:1409–1414
8. Zurek JR, Nadeson R, Goodchild CS. Spinal and supraspinal components of opioid antinociception in streptozotocin induced diabetic neuropathy in rats. Pain 2001;90:57–63
9. Chen SR, Sweigart KL, Lakoski JM, Pan HL. Functional mu opioid receptors are reduced in the spinal cord dorsal horn of diabetic rats. Anesthesiology 2002;97:1602–1608
10. Shangguan Y, Hall KE, Neubig RR, Wiley JW. Diabetic neuropathy: inhibitory G protein dysfunction involves PKC-dependent phosphorylation of Goalpha. J Neurochem 2003;86:1006–1014
11. Mousa SA, Cheppudira BP, Shaqura M, et al. Nerve growth factor governs the enhanced ability of opioids to suppress inflammatory pain. Brain 2007;130:502–513
12. Stein C, Schäfer M, Machelska H. Attacking pain at its source: new perspectives on opioids. Nat Med 2003;9:1003–1008
13. Gaveriaux-Ruff C, Nozaki C, Nadal X, et al. Genetic ablation of delta opioid receptors in nociceptive sensory neurons increases chronic pain and abolishes opioid analgesia. Pain 2011;152:1238–1248
14. Zöllner C, Mousa SA, Fischer O, et al. Chronic morphine use does not induce peripheral tolerance in a rat model of inflammatory pain. J Clin Invest 2008;118:1065–1073
15. Truong W, Cheng C, Xu QG, Li XQ, Zochodne DW. Mu opioid receptors and analgesia at the site of a peripheral nerve injury. Ann Neurol 2003;53:366–375
16. Yuyama K, Yanagisawa K. Late endocytic dysfunction as a putative cause of amyloid fibril formation in Alzheimer's disease. J Neurochem 2009;109:1250–1260
17. Yamdeu RS, Shaqura M, Mousa SA, Schäfer M, Droese J. p38 Mitogen-activated protein kinase activation by nerve growth factor in primary sensory neurons upregulates μ-opioid receptors to enhance opioid responsiveness toward better pain control. Anesthesiology 2011;114:150–161
18. Davidson E, Coppey L, Lu B, Arballo V, Calcutt NA, Gerard C, Yorek M. The roles of streptozotocin neurotoxicity and neutral endopeptidase in murine diabetic neuropathy. Exp Diabetes Res 2009:431980 Epub 2010 Feb 3.
19. Cahill CM, Dray A, Coderre TJ. Intrathecal nerve growth factor restores opioid effectiveness in an animal model of neuropathic pain. Neuropharmacology 2003;45:543–552
20. Luo MC, Zhang DQ, Ma SW, et al. An efficient intrathecal delivery of small interfering RNA to the spinal cord and peripheral neurons. Mol Pain 2005;1:29
21. Endres-Becker J, Heppenstall PA, Mousa SA, et al. Mu-opioid receptor activation modulates transient receptor potential vanilloid 1 (TRPV1) currents in sensory neurons in a model of inflammatory pain. Mol Pharmacol 2007;71:12–18
22. Shaqura MA, Zöllner C, Mousa SA, Stein C, Schäfer M. Characterization of mu opioid receptor binding and G protein coupling in rat hypothalamus, spinal cord, and primary afferent neurons during inflammatory pain. J Pharmacol Exp Ther 2004;308:712–718
23. Romero Rosales K, Peralta ER, Guenther GG, Wong SY, Edinger AL. Rab7 activation by growth factor withdrawal contributes to the induction of apoptosis. Mol Biol Cell 2009;20:2831–2840
24. Hellweg R, Lohmann P, Huber R, Kühl A, Riepe MW. Spatial navigation in complex and radial mazes in APP23 animals and neurotrophin signaling as a biological marker of early impairment. Learn Mem 2006;13:63–71
25. Zhao H, Laitala-Leinonen T, Parikka V, Väänänen HK. Downregulation of small GTPase Rab7 impairs osteoclast polarization and bone resorption. J Biol Chem 2001;276:39295–39302
26. Mousa SA, Shaqura M, Schäper J, et al. Identification of mu- and kappa-opioid receptors as potential targets to regulate parasympathetic, sympathetic, and sensory neurons within rat intracardiac ganglia. J Comp Neurol 2010;518:3836–3847
27. Yao X, Liu J, McCabe JT. Ubiquitin and ubiquitin-conjugated protein expression in the rat cerebral cortex and hippocampus following traumatic brain injury (TBI). Brain Res 2007;1182:116–122
28. Damke H, Baba T, Warnock DE, Schmid SL. Induction of mutant dynamin specifically blocks endocytic coated vesicle formation. J Cell Biol 1994;127:915–934
29. Brack A, Rittner HL, Machelska H, et al. Control of inflammatory pain by chemokine-mediated recruitment of opioid-containing polymorphonuclear cells. Pain 2004;112:229–238
30. Mousa SA, Shakibaei M, Sitte N, Schäfer M, Stein C. Subcellular pathways of beta-endorphin synthesis, processing, and release from immunocytes in inflammatory pain. Endocrinology 2004;145:1331–1341
31. Ohsawa M, Kamei J. Modification of kappa-opioid receptor agonist-induced antinociception by diabetes in the mouse brain and spinal cord. J Pharmacol Sci 2005;98:25–32
32. Zochodne DW, Verge VM, Cheng C, Sun H, Johnston J. Does diabetes target ganglion neurones? Progressive sensory neurone involvement in long-term experimental diabetes. Brain 2001;124:2319–2334
33. Piper RC, Katzmann DJ. Biogenesis and function of multivesicular bodies. Annu Rev Cell Dev Biol 2007;23:519–547

34. Hanyaloglu AC, von Zastrow M. Regulation of GPCRs by endocytic membrane trafficking and its potential implications. Annu Rev Pharmacol Toxicol 2008;48:537–568

35. Thibault D, Albert PR, Pineyro G, Trudeau LÉ. Neurotensin triggers dopamine D2 receptor desensitization through a protein kinase C and β–arrestin1-dependent mechanism. J Biol Chem 2011;286:9174–9184

36. Leterrier C, Bonnard D, Carrel D, Rossier J, Lenkei Z. Constitutive endocytic cycle of the CB1 cannabinoid receptor. J Biol Chem 2004;279:36013–36021

37. Ceresa BP, Bahr SJ. rab7 activity affects epidermal growth factor:epidermal growth factor receptor degradation by regulating endocytic trafficking from the late endosome. J Biol Chem 2006;281:1099–1106

38. Martini L, Waldhoer M, Pusch M, et al. Ligand-induced down-regulation of the cannabinoid 1 receptor is mediated by the G-protein-coupled receptor-associated sorting protein GASP1. FASEB J 2007;21:802–811

39. Bucci C, Thomsen P, Nicoziani P, McCarthy J, van Deurs B. Rab7: a key to lysosome biogenesis. Mol Biol Cell 2000;11:467–480

40. Vanlandingham PA, Ceresa BP. Rab7 regulates late endocytic trafficking downstream of multivesicular body biogenesis and cargo sequestration. J Biol Chem 2009;284:12110–12124

41. Balut CM, Gao Y, Murray SA, Thibodeau PH, Devor DC. ESCRT-dependent targeting of plasma membrane localized KCa3.1 to the lysosomes. Am J Physiol Cell Physiol 2010;299:C1015–C1027

42. Li J, Chen C, Huang P, Liu-Chen LY. Inverse agonist up-regulates the constitutively active D3.49(164)Q mutant of the rat mu-opioid receptor by stabilizing the structure and blocking constitutive internalization and down-regulation. Mol Pharmacol 2001;60:1064–1075

43. Apfel SC. Nerve growth factor for the treatment of diabetic neuropathy: what went wrong, what went right, and what does the future hold? Int Rev Neurobiol 2002;50:393–413

44. Kanbayashi H, Itoh H, Kashiwaya T, Atoh K, Makino I. Spatial distribution of nociceptive neuropeptide and nerve growth factor depletion in experimental diabetic peripheral nervous system. J Int Med Res 2002;30:512–519

45. Sasaki K, Chancellor MB, Phelan MW, et al. Diabetic cystopathy correlates with a long-term decrease in nerve growth factor levels in the bladder and lumbosacral dorsal root Ganglia. J Urol 2002;168:1259–1264

46. Cattaneo A. Tanezumab, a recombinant humanized mAb against nerve growth factor for the treatment of acute and chronic pain. Curr Opin Mol Ther 2010;12:94–106